Nanoscale Fluorescence Microscopy Using Carbon Nanotubes

Chun Mu, Benjamin D. Mangum, Changan Xie, and Jordan M. Gerton

(Invited Paper)

***Abstract*—We demonstrate the first reported use of single-walled carbon nanotubes as nano-optical probes in apertureless near-field fluorescence microscopy. We show that, in contrast to silicon probes, carbon nanotubes always cause strong fluorescence quenching when used to image dye-doped polystyrene spheres and Cd–Se quantum dots. For quantum dots, the carbon nanotubes induce very strong near-field contrast with a spatial resolution of ~20 nm. Images of dye-doped spheres exhibit crescent-shaped artifacts caused by distortions in the surface water layer found in ambient conditions.**

***Index Terms*—Atomic force microscopy (AFM), carbon nanotubes, fluorescence microscopy, fluorescence quenching, nano-optics, near-field optics.**

I. Introduction

BIOLOGICAL cells fabricate and assemble molecular building blocks into diverse molecular networks with striking complexity and functionality. Such networks are critical components in the complicated machinery of the cell, as they participate in a host of cellular functions including cell signaling and sensing, ion–channel gating, endo- and exocytosis, viral infection, as well as many other processes. Precise measurements of these networks will yield information that could create the ability to optimize specific cellular functions, to engineer new functions, and to strengthen a cell's defense against disease. Further, these networks are prototypical nanosystems and should be studied in detail for insight into the rational design of synthetic molecular systems for a multitude of technological applications. To study biological systems in this context, it is crucial to observe their molecular machinery at work in a physiologically relevant environment. Currently, there are no techniques that can accomplish this.

While electron microscopy, X-ray crystallography, and nuclear magnetic resonance spectroscopy can yield structural information with exquisite detail, these techniques are not suited for *in vitro* studies of complex molecular networks. In contrast, optical microscopy is minimally perturbative and is routinely used under physiological conditions. Fluorescence microscopy, in particular, is very powerful for studying biological systems because of its sensitivity to single molecules and the biochemical specificity afforded by modern conjugation methods. The major limitation of traditional optical microscopy is the limited resolution (~250 nm) imposed by classical light diffraction.

Recently, a number of far-field microscopy techniques have been developed to exceed the conventional diffraction limit, and even to obtain spatial resolution at the nanometer-length scale [1]. In 4-Pi microscopy, two microscope objectives are used in combination with coherent detection to effectively increase the numerical aperture, and thus, decrease the diffraction limit [2], [3]. Stimulated emission depletion (STED) microscopy beats the diffraction barrier by depleting the population of ground-state fluorophores except within the dark central region at the focus of a laser beam tailored to produce a doughnut-shaped intensity profile at the focus [4]. By increasing the intensity of the STED laser well beyond the saturation intensity, a subdiffraction volume of ground-state molecules is formed, which can then be probed using a low-intensity excitation laser with a Gaussian profile [1]. STED was the first of a host of far-field techniques, now also including ground-state depletion microscopy (GSD) [5] and saturated pattern excitation microscopy (SPEM) [6], which utilize photophysical transitions between bright and dark states to achieve subdiffraction resolution [1]. Other similar techniques utilize photochemical transitions between bright and dark states to achieve subdiffraction-limited resolution of either ensembles (RESOLFT) or even single molecules (PALM, STORM) [1], [7]–[9]. These techniques are not only a major step forward for nanoscale optical imaging of biological samples but also have some important limitations including the need for specially designed and synthesized fluorophores, the need for large laser intensities, which can lead to sample damage, and very slow image acquisition speeds, which can prohibit the study of dynamic biological processes.

Scanning-probe microscopy techniques such as atomic force microscopy (AFM) are powerful tools for nanoscale characterization of molecular-scale systems, since the sharp stylus can map extremely fine topographical variations on a sample surface. To minimize damage to soft samples, AFM can be operated in tapping or intermittent-contact mode: the cantilever probe is driven into rapid vertical oscillations, and the tip gently contacts the sample surface intermittently during each oscillation cycle. To form a topographical image, the AFM probe is raster scanned

Manuscript received September 30, 2007; revised October 27, 2007. The work of J. M. Gerton was supported by the Research Corporation under the Cottrell Scholar Award.

C. Mu, B. D. Mangum, and J. M. Gerton are with the Department of Physics, University of Utah, Salt Lake City, UT 84112 USA (e-mail: cmu@physics.utah.edu; bmangum@physics.utah.edu; jgerton@physics.utah.edu).

C. Xie was with the Department of Physics, University of Utah, Salt Lake City, UT 84112 USA. He is now with the Department of Biochemistry and Molecular Biology, Georgetown University, Washington, DC 20057 USA (e-mail: xieca@yahoo.com).

Color versions of one or more of the figures in this paper are available online at http://ieeexplore.ieee.org.

Digital Object Identifier 10.1109/JSTQE.2008.912914

across the surface, and variations in tip height are displayed as a function of the lateral position of the probe. AFM can be used to characterize the topographical structure of protein complexes and networks embedded in biological membranes *in vitro* [10]–[13]. Despite its utility, AFM cannot be used to identify distinct chemical species. Thus, AFM provides nanoscale resolution but no chemical sensitivity. Combining the attributes of AFM and optical microscopy leads to the intriguing possibility of obtaining both molecular-scale resolution and chemical specificity.

In this paper, we describe recent progress toward nanoscale imaging of biomolecular systems using apertureless near-field scanning optical microscopy (ANSOM), a technique that combines the AFM and optical microscopy. In particular, we demonstrate that both the resolution ($\sim$10 nm) and sensitivity of ANSOM make it promising for imaging molecular-scale biological systems *in vitro*. Further, we report the first use of single-walled carbon nanotubes as nano-optical probes in fluorescence microscopy.

II. Apertureless Near-Field Microscopy

In conventional near-field scanning optical microscopy (NSOM), the optical-diffraction barrier is overcome by forcing light through a nanoscale aperture at the end of a sharp tip that is maintained in close proximity to a surface [14], [15]. NSOM can be used to measure the nanoscale organization and orientation of biological molecules on surfaces and in membranes [16]. Although 30 nm resolution is theoretically possible, resolution below 50 nm is seldom seen due to the severe cutoff in light transmission efficiency for small apertures [17]. ANSOM circumvents this limit by replacing the small aperture with a sharp tip such as an AFM probe in the focus of a laser beam. The nano-optical field in the vicinity of the tip apex can be strongly enhanced due to the resonant excitation of localized surface plasmons [18], or to geometric considerations such as the lightning-rod effect [17], [19], [20] or the antenna effect [21], [22]. The tip-enhanced field can be used to locally excite various optical processes such as fluorescence, Raman scattering, and elastic (Rayleigh) light scattering, and has resulted in several reported measurements of spatial resolution below 30 nm [23]–[32], including one report on the use of a carbon nanotube bundle to visualize the plasmon fields of gold nanodisks using elastic light scattering [33]. High-resolution fluorescence microscopy can also be used to obtain information on the orientation of fluorophores via the overlap of the excitation dipole moment with the local optical field direction [16], [25], [34]–[36].

Near-field contrast can also be obtained if the tip causes a local reduction in the detected signal, either by redirecting the fluorescence emission away from the detection solid angle via coupling to the induced tip dipole [34], or by optical energy transfer to the tip (fluorescence quenching) [37]–[39]. These effects are generally very short range ($<$20 nm), providing nanoscale-resolution capabilities. Tip-induced reduction of fluorescence can be used to study important nanoscale phenomena such as the energy transfer and dissipation mechanisms, both in synthetic and in biological systems.

The primary advantage of ANSOM compared to conventional aperture-type NSOM is that it can achieve resolution that is limited primarily by the tip sharpness to just a few nanometers [24]. On the other hand, ANSOM suffers from an increased background due to direct excitation by the laser. Thus, to achieve the sensitivity needed to image dense samples such as biological systems, it is very important to optimize the near-field contrast. This can be done by engineering the geometric and material properties of the tip to yield the largest field enhancement [40]. In particular, specific tip geometries that leverage antenna and lightning-rod effects, or that support plasmon resonances at the distal end, can produce very-large-field enhancements, and thus, very high sensitivity, both for imaging and sensing applications. In addition, metallic probes generally yield higher field enhancement than geometrically equivalent dielectric probes, but they can also cause fluorescence quenching, which generally dominates field enhancement at very small tip–sample separations [39].

Recently, the benefits of the ANSOM and aperture-type NSOM have been combined by fabricating a nanoscale metal tip on the periphery of an aperture-type probe [23], [41]. The tip is illuminated through the aperture, instead of via a focused laser, which greatly reduces the background. The light emerging from the aperture excites surface plasmons that travel from the base to the end of the tip, where they are reconverted to light. These tip-on-aperture probes were used to image individual fluorescent molecules dispersed on a glass surface with $\sim$25 nm resolution. More recently, it has been shown that the metal tip acts as a $\lambda/4$ monopole antenna whose efficiency depends on length [22]. For both cases, each probe was fabricated using rather complicated techniques such as focused ion beam milling or electron beam deposition. Carbon nanotubes may provide an interesting alternative for the tip-on-aperture, approach since they have unique electronic and optical properties and have small diameters [42]. Furthermore, they can be lifted off a substrate directly by an AFM probe, and can then be repeatedly shortened to precise lengths using simple procedures (see following sections) [43], [44].

A. Tip-Enhanced Fluorescence Microscopy

We developed an ANSOM technique called tip-enhanced fluorescence microscopy (TEFM) that combines AFM with confocal fluorescence microscopy (see Fig. 1). Briefly, a silicon AFM tip is positioned into the focus of a laser beam. We find that silicon tips generally yield the largest net fluorescence enhancement because, unlike metal tips, they do not induce quenching [37]–[39]. Using quantum dots to probe the optical intensity near silicon tips, we measured an increase in the fluorescence rate of up to a factor of $\sim$20 relative to the far-field background. This enhanced fluorescence rate decays to the far-field level when the tip is retracted from the sample by 5–20 nm depending on the sharpness of the tip and the size of the fluorescent particle [24], [25].

To generate strong enhancement, the optical field must be polarized parallel to the long axis of the tip at the focus. We use either a laser-beam mask or a radial polarization generator

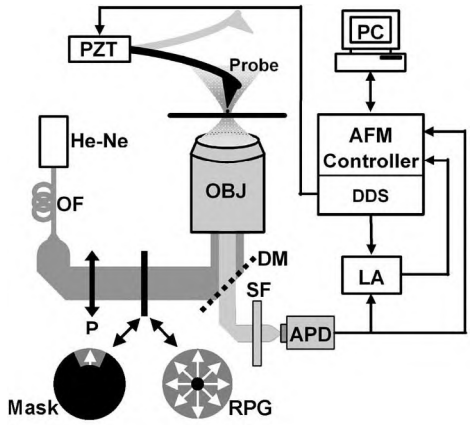

Fig. 1. Experimental setup for ANSOM. Labeled elements are as follows: He-Ne: helium-neon laser; OF: optical fiber; P: polarizer; Mask: laser-beam mask; RPG: radial polarization generator; DM: dichroic mirror; OBJ: microscope objective; Probe: AFM probe; PZT: piezoelectric transducer; SF: spectral filters; APD: avalanche photodiode; LA: lock-in amplifier; DDS: digital synthesizer; PC: personal computer. The white arrows indicate the instantaneous polarization state after the laser beam has passed through either the beam mask or the RPG.

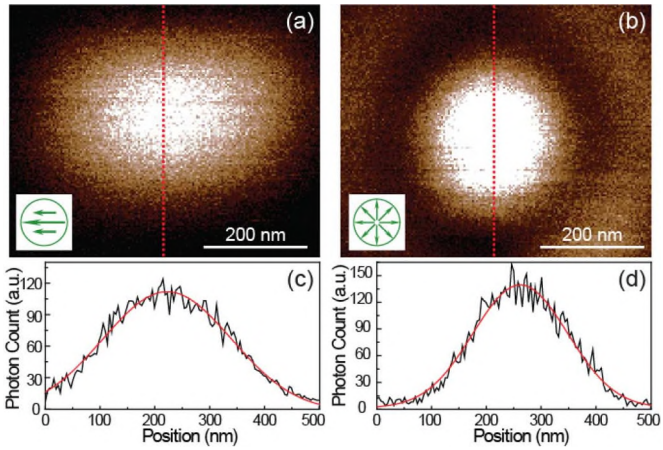

Fig. 3. Fluorescence images of 20-nm diameter polystyrene beads under two different excitation laser modes as indicated by the insets: (a) shows a diffraction limited spot for linear polarization. (b) shows radial polarization. The corresponding cross sections with Gaussian fits are shown in (c) and (d). Widths of the Gaussian fits are: 234 ± 12 nm for linearly polarized laser and 172 ± 5 nm for radially polarized laser.

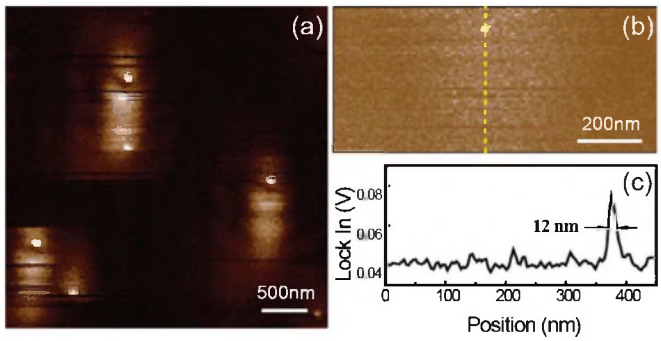

Fig. 2. TEFM images of quantum dots on a glass surface using a silicon AFM probe. (a) Fluorescence image of several isolated quantum dots with no lock-in amplification. The elongated shape of the far-field fluorescence background results from using the focused-TIRF illumination scheme. The size of the far-field spot is about 1 μm $\times$ 0.5 μm. (b) Lock-in magnitude image of an isolated quantum dot. (c) Profile specified by dashed line in (b).

(RPG) to produce the requisite axial field. The beam mask produces an axially polarized evanescent field above the glass–air interface within a relatively tight focal spot (1 μm $\times$ 0.5 μm), as shown in Fig. 2(a). We call this illumination scheme focused total internal reflection fluorescence (TIRF), because it is similar to conventional TIRF microscopy, except that the illumination is confined to a small focal area rather than a wide field. The RPG generates a radially polarized laser beam (TEM_{01*}) from a standard linearly polarized TEM_{00} mode. The requisite axially polarized field is created when the TEM_{01*} mode is focused tightly using a high numerical aperture objective [35], [45]. Furthermore, the TEM_{01*} mode produces a smaller focus spot compared to a standard TEM_{00} mode, as shown in Fig. 3. TEFM typically requires very low optical powers ($\sim$200 nW) due to the tight laser focus, strong spectral rejection of nonfluorescent background signals, and high overall detection efficiencies (10%–20%).

One important issue in TEFM is the presence of far-field fluorescence background. At high fluorophore densities, multiple molecules within the laser focus elevate this background, while the tip-enhanced signal remains unchanged, since the enhanced-field volume is so small. Thus, the TEFM SNR decreases when the fluorophore density increases. In general, radially polarized illumination is preferable because, it produces the smallest focus spot. In practice, we sometimes use focused TIRF illumination, because it is simpler to implement. Further, it may be the preferred illumination scheme for imaging in water, since it produces a relatively tight focal area whose intensity decays exponentially above the glass–water interface. This may reduce additional background signal originating from fluorophores diffusing into the focal volume.

One way to suppress background fluorescence independent of the illumination scheme is to operate AFM in tapping mode. This oscillatory motion modulates the local fluorescence signal, as the probe intermittently contacts the surface, transiently elevating the local fluorescence rate, and then, withdraws, whereupon the signal returns to the background rate. Subsequent demodulation at the probe oscillation frequency suppresses the background, leading to high-fidelity images with resolution limited only by the sharpness of the tip. We recently demonstrated $\sim$10 nm resolution in TEFM images of isolated quantum dots dried onto glass coverslips [24], [26]. Furthermore, we have imaged fluorescent "dumbbells" composed of short DNA oligomers (60 base pairs) end labeled with Cy3 fluorophores at a resolution of $<$10 nm [24], [25]. Finally, we have shown that high-density samples of quantum dots can be imaged with good contrast while maintaining $\sim$10 nm resolution [24], [26]. Fig. 2 shows sample images of isolated quantum dots in air obtained using focused TIRF illumination: Fig. 2(a) shows the fluorescence signal before demodulation, while Fig. 2(b) shows the fluorescence signal of a single quantum dot after demodulation using a commercial lock-in amplifier.

B. Fluorescence Reduction

As discussed before, metal tips can induce a reduction in the fluorescence rate, since they can nonradiatively dissipate the excitation energy of nearby fluorophores [39]. This energy transfer process called fluorescence quenching leads to a reduction in the excited-state lifetime of the fluorophores, which can be measured directly using pulsed lasers and time-correlated single-photon counting [37], [38]. Furthermore, the detected fluorescence rate can also be reduced due to the coupling of the fluorophore emission dipole to the induced dipole in the tip [34]. This can cause a redirection of the fluorescence emission into angular regions that are not detectable with the microscope objective from below (see Fig. 1). Both reduction mechanisms are dependent on the orientation of the fluorophore dipole moments with respect to the long axis of the tip, and thus, can be used to decode the molecular orientations. Further, since these mechanisms act over a very short range, they can be used to generate high-resolution images of a fluorescent sample, either by measuring the reduction of fluorescence rate or the reduction in lifetime. Fluorescence quenching is particularly interesting as an energy transfer mechanism, and measuring the precise spatial dependence helps reveal the mechanistic details [39]. In quenching, the excitation energy of the fluorophore is transferred to electronic excitations in the metal, which are then dissipated via Ohmic loss processes. Thus, the quenching efficiency is ultimately proportional to the imaginary part of the dielectric function, which, for metals, can be relatively large, yet for dielectrics can be very nearly zero: at 600 nm, the imaginary part of the dielectric function is 1.366 for Au [46], [47], 0.104 for Si [48], [49], and zero for crystalline SiO_2 (quartz) [47]. The quenching efficiency is also dependent on the geometry of the tip [39].

Although quenching can be used to modulate the fluorescence rate, demodulation schemes, particularly, lock-in amplification, are generally not very effective for tip-induced quenching as compared to tip-induced enhancement. This arises from the fact that a lock-in amplifier produces a large signal only if detected photons are clustered within a narrow phase-window of the AFM-probe oscillation cycle, thereby producing a well-defined phase for the lock-in algorithm. In the case of quenching, there is a reduction in the number of photons when the tip contacts the sample, and there is no well-defined lock-in phase. Thus, if the AFM is operated in tapping mode, the overall contrast is reduced, since the fluorophores spend less time within the quenching region of the tip. In addition, when imaging relatively large fluorescent particles, the contrast is further reduced, since only a fraction of the particle volume overlaps with the quenching region near the tip. Fig. 4 shows typical images of both polystyrene beads and quantum dots when imaged with metal AFM tips in comparison to the contrast achieved by fluorescence enhancement when using a silicon tip.

Despite the loss of contrast, it is usually important to operate the AFM in tapping mode for a number of reasons. First, the AFM probe maintains its sharpness much longer, and is less destructive to soft samples when it contacts the surface only intermittently. Second, although lock-in amplification is not an ideal demodulation algorithm in the case of fluorescence quenching, there are more sophisticated algorithms that can be applied which exceed the SNR of simple photon summing. We have developed a novel phase-sensitive photon counting technique in which photon arrivals are permanently recorded in terms of the instantaneous phase of the probe oscillation cycle. With this data acquisition technique, arbitrary analysis algorithms can be applied offline to the data on a per photon basis. We are currently using the Monte–Carlo simulations of our experiment to develop analysis algorithms that optimize the SNR for the case of fluorescence quenching.

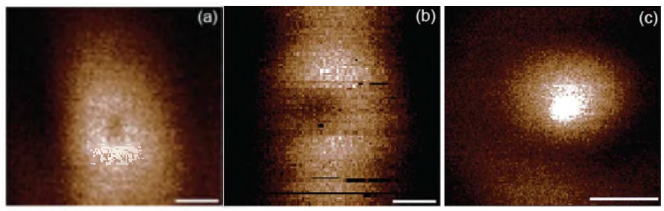

Fig. 4. (a) Fluorescence images of a polystyrene bead and (b) quantum dot when using Cr/Pt coated AFM probe. Signal reductions are observed in both the cases. By comparison, (c) the fluorescent signal of a polystyrene bead is strongly enhanced while using a silicon probe. Scale bars are 200 nm.

III. Carbon Nanotubes

Carbon nanotubes (CNTs) are prototypical 1-D systems whose unique mechanical, electrical, and optical properties make them intriguing for use as topographical probes, optical probes, or antennas in various scanning probe and nano-optical applications especially the ANSOM [50]–[55]. In recent years, a number of techniques for attaching nanotubes to AFM probes have been developed, enabling individual nanotubes to be manipulated and positioned with nanometer-scale precision [43], [44], [56]–[63]. The attached nanotubes are generally stable, and, due to their small diameters (1–10 nm) and high axial stiffness [64], [65], they exhibit very fine resolution in scanning probe microscopy applications [44]. Once attached, the nanotubes can be shortened in precise steps from micrometers to nanometers, enabling optical measurements with a single, well-characterized probe [43]. Finally, due to their 1-D nature, nanotubes exhibit novel plasmonic mode structure, which may lead to efficient optical energy transfer across a wide energy spectrum, and thus, a reduction in the detected fluorescence.

A. Fabrication and Characterization

In order to use nanotubes as probes for either topographical or optical studies, they must be robustly attached to an AFM tip. Although nanotubes can be grown directly onto tips using chemical vapor deposition (CVD) [66], we use the so-called pickup method [43]. In this technique, nanotubes are lifted off a CVD-grown substrate by an AFM tip via Van der Waals interactions, as the tip is scanned over the nanotube-coated surface. In general, the attached nanotubes are too long for useful AFM imaging because of thermal vibrations at the distal end of the nanotube (see Fig. 6). Further, long nanotubes tend to elastically

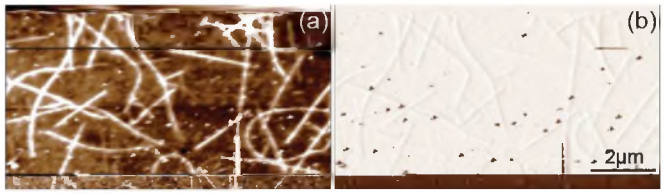

Fig. 5. AFM images of a nanotube-covered silicon wafer. The images were obtained as the probe was scanned from top to bottom: panel (a) shows the AFM topography signal and panel (b) shows the AFM phase signal. Resolution increased dramatically when a CNT was picked up, while the phase suddenly changed.

buckle when loaded axially (see Fig. 7). Thus, the nanotubes usually must be shortened significantly to a protrusion length of <100 nm.

There are two simple techniques for shortening nanotubes attached to AFM probes: push shortening and pulse shortening. In push shortening, an attached nanotube can be slid up the side of an AFM tip simply by pushing the distal end onto a hard surface [44]. This technique works well for nanotubes below $\sim$200 nm in length and can produce extremely precise ($\sim$2 nm) shortening steps. For longer nanotubes, the push shortening method generally fails, since the nanotubes will usually buckle elastically rather than slide up the tip sidewalls. In this case, pulse shortening must be employed, wherein short voltage pulses are applied between the AFM probe and a conductive substrate. The electrical pulses tend to ablate carbon layers from the distal end of the nanotube. Controlling the voltage and duration of the pulses can alter the shortening steps. In this manner, many small voltage pulses can be applied until the nanotube reaches the desired length [67].

Our carbon nanotubes were grown on silicon substrates using the CVD method [67], and are attached to commercially available silicon AFM probes (Budget Sensors Multi-75) via the pick-up method [43]. During the pick-up procedure, AFM probes are used to image the growth substrate, and there are two main indicators for successful pick up. First, there is often a dramatic change in image resolution, as shown in Fig. 5(a). This increase in resolution is due to the fact that CNTs are in general sharper and have higher aspect ratio than AFM probes. A more robust indicator of nanotube pick up is an instantaneous change in the oscillation phase of the AFM probe, as shown in Fig. 5(b). Regardless of the length of the nanotube that adheres to the AFM probe, the phase image always shows a change in contrast due to the sudden change in the probe–sample interaction forces. After the pick up, only a few more lines are scanned to ensure that the CNT is firmly attached and to avoid picking up additional nanotubes.

Fig. 6 shows an SEM image of a carbon nanotube attached to a commercial silicon probe before shortening. It is not efficient to use the SEM to measure the nanotube length during the shortening procedure. However, the nanotube length can be measured *in situ* using approach curves: the AFM tip is lowered onto a hard substrate (e.g., Si), and the deflection of the soft cantilever is monitored. When the nanotube touches the surface, a "kink" in the approach curve appears before the nanotube buckles elastically under the axial load. Several buckling transitions can occur as the tip is lowered further until finally the silicon tip snaps to contact. Beyond this point, the cantilever deflection becomes linear. The distance between the initial kink caused by nanotube contact and the contact point of the silicon tip provides a repeatable measure of the nanotube length. This method can be applied during the shortening procedure to monitor the intermediate length of the nanotube. Fig. 7 shows an approach curve before the shortening procedure (top curve) and after (bottom curve).The initial length of the nanotube was $\sim$440 nm, and after the application of several 20 V pulses ($\sim$10 μs duration), the nanotube is shortened to $\sim$30 nm.

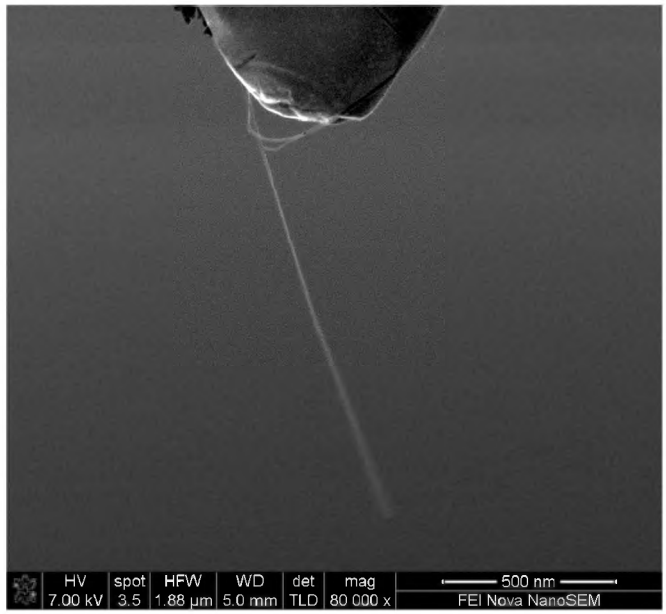

Fig. 6. Field emission scanning electron micrograph of CNTs attached to a silicon AFM probe. In this case, there are a few nanotubes attached to the probe apex. Thermal vibration at the distal end of the long nanotube can be seen in the image.

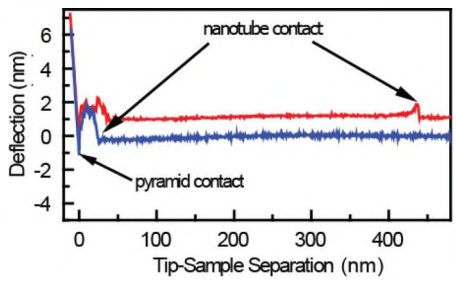

Fig. 7. AFM approach curves of a CNT-probe before shortening (top curve) and after shortening (bottom curve). There is a kink in the cantilever deflection signal when the nanotube touches the surface, as indicated. The distance between these kinks and where the pyramid contacts gives the length of the nanotube: $\sim$440 nm before shortening and $\sim$30 nm after shortening in this case.

B. AFM With Nanotubes

After attachment and shortening, the nanotubes can then be used as AFM probes, whose resolution should reflect the diameter of a nanotube tip. However, there are a number of effects that

can either increase or decrease the resolution. First, after pulse shortening, the nanotubes should be open ended, and thus, are very pliable along the radial direction. Atomistic simulations of this system have predicted that this can lead to finer resolution than predicted by the tube diameter, as the tube deforms, and thus, narrows its profile as it scans over an object [68]. On the other hand, there is also evidence that a thin water layer that forms on the surface of all the samples will increase the width of the AFM images under some circumstances [69]. Finally, it is unlikely that the attached nanotube protrudes in a precisely vertical direction from the AFM probe. This can lead to imaging artifacts that effectively decrease the resolution.

The growth and attachment procedure outlined before should yield nanotube diameters below 10 nm [44]. We have used the nanotube probes to image a variety of samples, including dye-doped polystyrene spheres (nominal diameter: ~20 nm), fluorescent Cd–Se quantum dots (nominal size: 4 nm × 9.4 nm ellipsoids), and other nanotubes lying prone on silicon substrates. For example, when imaging the 20-nm polystyrene spheres, we typically observe full widths of 60–100 nm in the AFM height trace [see Fig. 9(a) and (f)]. Similar image broadening has been observed previously when using nanotube tips [69]. The model proposed to describe this phenomenon in ambient conditions is that nanoscale particles tend to deform the water layer in a manner that leads to a thickening of the water layer along the particle sides that extends outward for several tens of nanometers. It is expected that the water layer acts as a penetration barrier for nanotubes due both to the surface tension and the fact that nanotubes are generally considered to be hydrophobic. Thus, images formed using nanotube probes often exhibit widths that are substantially broadened; since under some circumstances, the nanotubes follow the surface of this thickened water layer, rather than the particle itself. This model is consistent with our measurements on polystyrene spheres.

The deformed water-layer model also suggests that the thickness of the water layer on top of the particle may be thinner than on the flat supporting substrate. There is some evidence of this in the phase trace of the polystyrene sphere shown in Fig. 9(c) and (h). Even though the height trace [see Fig. 9(a) and (f)] exhibits a broadened width, the full width of the phase trace is 26 nm along the fast axis and 23 nm on the slow axis (data not shown). The dark (low) phase values indicate a net repulsive interaction between the tip and sample, which could arise if the nanotube distorts the water layer to the degree that it feels a hard-contact repulsion from the sample surface. Alternatively, low phase values could simply indicate an increase in repulsive interactions upon nanotube penetration into the water layer. Finally, there has been a suggestion that the hydrogen bonding within ultrathin water layers can actually lead to icelike behavior [70], in which case, the repulsive interactions would be expected to increase. All of these explanations are more likely if the water layer is thin. Thus, our observations are evidence that the water layer on top of the sphere is thinner than on the flat supporting substrate. Interestingly, for small objects, this effect is not observed: Fig. 8(c) shows that the phase and height images for ~4 nm diameter quantum dots do not differ significantly in their spatial extent. This may be an indication that the

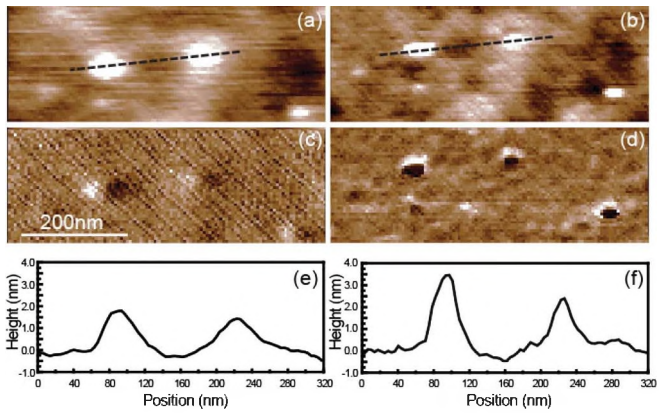

Fig. 8. AFM topography images of quantum dots. Panel (a) corresponds to a probe oscillation amplitude of 12 nm and panel (b) corresponds to an amplitude of 26 nm. For the same quantum dot, the height increases from 1.9 nm to 3.5 nm as the amplitude is increased, as shown in (e) and (f). Corresponding phase images are shown in (c) and (d) for small and large amplitudes respectively.

absolute thickness of the water layer on the top of larger objects is thinner as compared to the absolute thickness on top of the smaller objects. Since the penetration of the nanotube occurs only on the top of the sphere, where the water layer is thinner, the dark (low) phase region is a likely indicator for the true size and location of the sphere.

The difference in water layer thickness could also lead to AFM images with measured heights that are artificially smaller than the true height. Quantum dots are very useful for testing this, since they are small, hard, and since the spectral characteristics of their emission guarantees a particular diameter. If we image the quantum dots using a small oscillation amplitude (i.e., low energy in cantilever motion), the images exhibit a height that is markedly smaller than the known value, as shown in Fig. 8(a) and (e). On the other hand, when a larger amplitude is employed, the cantilever now has enough energy to penetrate the water layer, and the measured height is more consistent with the true value, as shown in Fig. 8(b) and (f). These two situations also exhibit significant differences in their phase behavior, as shown in Fig. 8(c) and (d), indicating a transition in the tip–sample interaction as discussed before. The difference in measured heights for the two cases provides a measure of the difference in water layer thickness on the top and sides of the quantum dots, which is ~1.6 nm in this case. Regardless of the amount of energy in the cantilever motion (i.e., its amplitude), for relatively large particles, a close approximation of the true height of the sample can be obtained because the fractional error introduced by the difference in water layer thicknesses on the top and sides of the object is quite small. This is not valid for particles of size on the same scale as the water layer thickness (a few nanometers), and the true height can only be obtained by increasing the oscillation amplitude to penetrate the water layer. This is problematic for small soft samples that may be easily deformed by the tip, in which case, the true height may not be easily obtained in any imaging mode under ambient conditions. Interestingly, this effect should

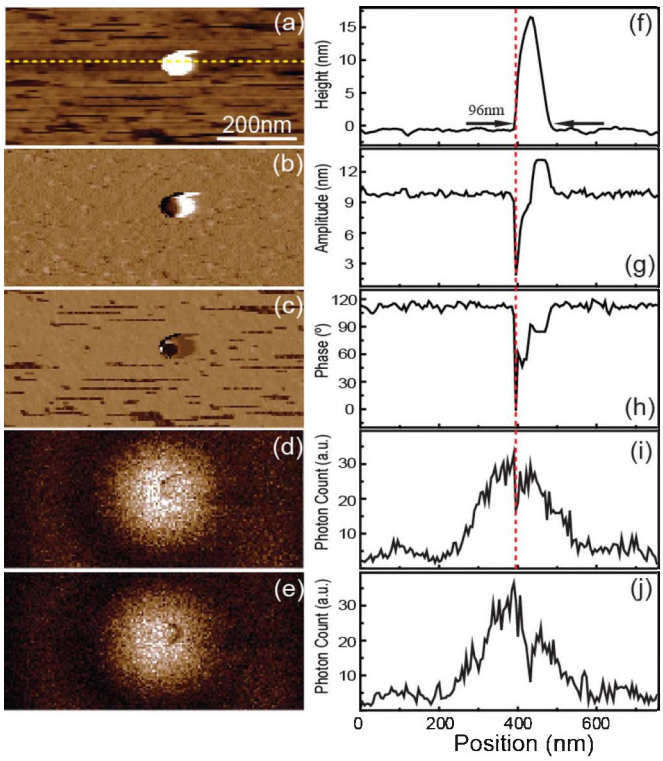

Fig. 9. AFM and TEFM images of a dye-doped polystyrene sphere using a CNT probe. Panels (a)–(c) show AFM topography, amplitude, and phase signals, respectively, for a left-to-right movement (trace) of the CNT probe. Panels (d) and (e) show TEFM signals for the trace and retrace movements of the probe, respectively. All data were obtained simultaneously. The right column shows the corresponding signal profiles for these images along the horizontal dashed line in (a). The vertical dashed line in (f) through (i) shows the correlation between the minimum AFM oscillation amplitude, the maximum reduction in fluorescence, and the minimum value for the phase.

be absent when the entire sample and tip are immersed under water.

The surface water layer discussed here should be present for any sample under ambient conditions. In fact, this water layer provides the mechanism needed for effective shear-force feedback widely used in aperture-type NSOM [71]. The specific structure of the water layer is not determined by the tip, but rather by the substrate, sample, temperature, and humidity [69], [70], [72]–[78]. Thus, when using an AFM probe without a nanotube, this width broadening would also be expected, assuming that the energy in the tip is low, i.e., small amplitudes. Width broadening with regular AFM tips, while not unnoticed, is hard to characterize. For example, a typical AFM image that appears broadened, but that exhibits a reasonable height, may be attributed to simply a fat or dulled tip. Carbon nanotubes are unusually sensitive to artifacts caused by the surface water layer, since they have high aspect ratios, small diameters, and are generally considered to be hydrophobic. Increasing the cantilever free amplitude or decreasing the ratio of the amplitude set point relative to the free amplitude, can give the probe enough energy to penetrate the water layer as it approaches the sample, as shown in Fig. 8 [69]. Furthermore, imaging in a dry environment (e.g., N_2 or Ar) or under vacuum should reduce or eliminate the artifacts caused by the water layer. Other imaging artifacts, such as a narrowing of the AFM image caused by the deformation of the nanotube as it scans over a small object [68], [79], are also possible. Evidently the importance of various artifacts depends on the imaging and/or environmental parameters.

C. ANSOM With Nanotubes

The ability of the nanotube to penetrate the water layer will obviously affect its ability to either enhance or quench the fluorescence. If the nanotube is not able to penetrate the water layer, then its average distance from the fluorescent particle will be larger, and the spatial overlap between the enhancement or quenching region and the volume of the particle will decrease. In this case, we might expect a reduction in the near-field contrast. On the other hand, if the nanotube is able to penetrate the water layer, we might expect strong near-field contrast. Furthermore, if the tip oscillation amplitude is strongly damped when the nanotube is in the nanoscale vicinity of the particle, then the average separation between the nanotube and the particle will be smaller, and we might expect an increase in near-field contrast.

Fig. 9 shows AFM and optical signals for a nanotube tip imaging a fluorescent polystyrene sphere with nominal diameter of ~20 nm. Panels 9(a)–(d) and their corresponding profiles 9(f)–(i) correspond to a fast scan axis moving from left to right (trace), while panels 9(e) and (j) correspond to a fast axis moving from right to left (retrace). As seen in Fig. 9(a) and (f), the AFM height trace exhibits a full width of nearly 100 nm. This width broadening is in part due to the water layer phenomenon discussed before, and in part to the AFM feedback loop's inability to follow the precise contours of the sphere. Although the height trace exhibits width broadening, the measured height of the bead is ~18 nm, in fair agreement with its nominal diameter, but probably reduced somewhat due to the difference in thickness of the water layer between the glass substrate and top of the sphere. From Fig. 9(d) and (e), we observe that within the background fluorescence spot, there is a crescent of reduced fluorescence in both the trace and retrace. At precisely the same time and location that the minimum of fluorescence occurs, there is a dramatic reduction in both the phase and amplitude of the probe oscillation.

The first thing to note is that there is no evidence of fluorescence enhancement in these images. Rather, the fluorescence is strongly suppressed within the crescent-shaped region. We have made similar measurements on several hundred fluorescent particles, both dye-doped spheres, as in Fig. 9, and CdSe–ZnS quantum dots, as in Fig. 10, using more than 50 different nanotube probes. In each and every case, enhancement is consistently absent. This is, at first, somewhat puzzling, because we expect the nanotube growth and attachment procedure described before to yield a mixture of metallic and semiconducting nanotubes. While we may expect metallic nanotubes to quench fluorescence, we also might expect that semiconducting nanotubes would strongly enhance fluorescence due to their geometry and the lack of dissipative electronic modes. One must keep in mind, however, that the bandgap of semiconducting

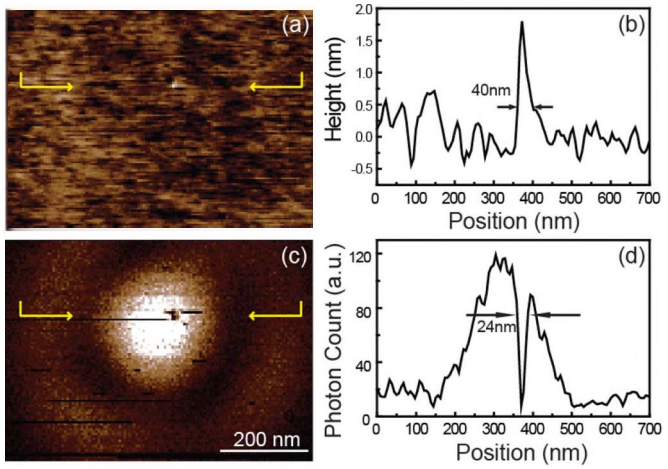

Fig. 10. AFM and TEFM images of a CdSe/ZnS quantum dot using a CNT probe. Panel (a) shows the AFM topography signal and panel (c) shows the TEFM signal. Corresponding signal profiles are shown in the right column in panels (b) and (d) respectively. A reduced height of 2 nm for the quantum dot was observed as shown in (b). The AFM amplitude gets damped only slightly, a 10% decrease of the set-point at the leading edge of the quantum dot (data not shown).

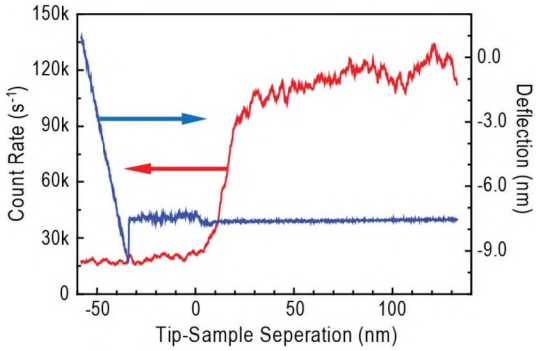

Fig. 11. AFM approach curve on top of a quantum dot using a CNT-tip. Blue curve is the AFM-cantilever deflection, where the small "kink" indicates where the CNT touches the surface. The fluorescence signal was recorded simultaneously, as shown in red. The photon count rate dramatically dropped from ~120 to ~16 kcounts/s within 25 nm.

nanotubes (<1 eV) is far below the energy of both excitation and fluorescence photons in our experiment. Thus, there may be photoinduced charge carriers that can dissipatively quench fluorescence as if they were metallic. This argument is not, however, altogether consistent with previous observations, since the bandgap of silicon (1.1 eV) is also far below the photon energies, and all of the hundreds of silicon probes tested over several years only exhibit evidence of enhancement. The difference in behavior between nanotubes, some of which are expected to be semiconductors, and silicon tips is very interesting, and may be a consequence of the 1-D nature of the nanotubes. We plan to explore this issue at length in an upcoming publication.

The quenched fluorescence crescent is a direct consequence of the drop in oscillation amplitude. This abrupt decrease of amplitude is most likely the result of the nanotube probe coming into contact with a positive edge, which transiently damps the probe oscillation. When the probe oscillation amplitude is small, the time that the fluorescent bead stays inside the quenching region increases, and the contrast (i.e., SNR) is strong. The other factor affecting quenching is the quenching volume overlap. From purely geometrical considerations, this overlap is maximal when the nanotube is displaced laterally from the bead. It has been shown previously that effective quenching of quantum dots [80] and molecular fluorophores [81], [82] can be caused by the sidewalls of a nanotube. This combination of effects leads to maximum quenching along the leading edge of the distorted water layer. Little or no quenching is observed as the nanotube scans over the top surface of the bead because the quenching volume overlap is relatively small, and the oscillation amplitude is increasing. Within this model, the size and shape of the quenched crescent essentially map out the leading edge of the distorted water layer. Using the photon count trace and retrace images, the crescent measures ~50 nm from tip to tip. Thus, in this case, the distortion in the water layer appears to persist 10–20 nm beyond the edge of the sphere.

In Fig. 10, we show an AFM height trace with the corresponding near-field optical image of a quantum dot. Again, we find that the width of the quantum dot is far larger than expected and the height is reduced, both indicating that the energy in the cantilever is not sufficient to penetrate the distorted water layer in order to contact the particle. Here, we note almost complete quenching of the quantum dot in a disk shape, rather than a crescent. In fact, in over 100 images of quantum dots, we have never observed a quenched crescent. This is likely the case because the distortion in the water layer for the small quantum dot is not sufficient to strongly damp the probe oscillation at the leading edge.

We can obtain additional information about the length scale of fluorescence quenching by measuring approach curves, whereby the cantilever oscillation and lateral scanning motion are stopped and the nanotube is precisely lowered onto a quantum dot from a particular height. We have measured many approach curves using more than 10 different nanotube tips on top of many different quantum dots. In all cases, the quenching starts 15–25 nm away from the quantum dot, as shown in Fig. 11. The point at which the nanotube touches the quantum dot is indicated by the kink in the cantilever deflection signal, as discussed before.

In Fig. 10, the peak-to-peak oscillation amplitude of the probe was ~24 nm, slightly larger than the quenching interaction length shown in Fig. 11. Thus, we expect that the distal end of the nanotube spends a significant portion of its oscillation cycle outside the region of strong quenching. This should tend to reduce the contrast, as the fluorescence rate is averaged over the entire oscillation cycle. However, in Fig. 10, we observe essentially complete quenching over the area of the quantum dot. This may be an indication that quantum dots need some time to recover following a quenching interaction. This could be the result of charge transfer between the quantum dot and nanotube, since the diffusion of excitonic electrons into the ZnS shell is known to cause a reduction in nanocrystal quantum efficiency [83]. The oscillation frequency of the AFM probe, in this case, is ~75 kHz, so the recovery timescale would have to be longer than ~10 μs. We will investigate this issue in the

future using time-resolved measurements. If charge transfer is important in this case, it has strong implications for the potential use of nanotube–nanocrystal composites in photovoltaic and photosensor applications.

IV. Conclusion and Future Directions

We have demonstrated that carbon nanotubes can be used for nanometer-scale imaging of fluorescent samples. Somewhat surprisingly, the nanotubes do not induce fluorescence enhancement, in stark contrast to silicon AFM probes. Rather, all nanotubes tested (>50) produced strong fluorescence quenching, despite the fact that we expect a mixture of metallic and semiconducting nanotube tips. The difference in behavior between silicon AFM tips and nanotubes may be a consequence of the 1-D nature of charge and energy transport in nanotubes. We plan to explore this issue through careful spatial measurements of the quenching efficiency using pulsed lasers to measure the lifetime directly.

Carbon nanotubes were also found to be extremely sensitive to distortions in the surface water layer present on all samples under ambient conditions. This water layer leads to a width-broadening effect in tapping-mode AFM with nanotube tips and to other topographical artifacts including reduced height traces. Further, the water layer leads to crescent-shaped optical images of 20-nm diameter fluorescent beads, but not for the more compact quantum dots. In the future, we will investigate the use of carbon nanotubes to image samples under water, for which the water layer effects should be absent. This could lead to nanoscale imaging of biological systems *in vitro*.

Finally, optical images of quantum dot quenching provide a subtle hint of charge transfer between quantum dots and nanotubes. We will investigate this possibility by measuring the temporal delay of fluorescence recovery following a quenching event. Confirmation of charge transfer would have important implications for the use of nanotube–nanocrystal composites in photovoltaic and photosensor applications.

References

[1] S. W. Hell, "Far-field optical nanoscopy," *Science*, vol. 316, pp. 1153–1158, 2007.

[2] S. W. Hell and E. H. K. Stelzer, "Fundamental improvement of resolution with a 4Pi-confocal fluorescence microscope using two-photon excitation," *Opt. Commun.*, vol. 93, pp. 277–282, 1992.

[3] H. Gugel, J. Bewersdorf, S. Jakobs, J. Engelhardt, R. Storz, and S. W. Hell, "Cooperative 4Pi excitation and detection yields sevenfold sharper optical sections in live-cell microscopy," *Biophys. J.*, vol. 87, pp. 4146–4152, 2004.

[4] T. A. Klar, E. Engel, and S. W. Hell, "Breaking Abbe's diffraction resolution limit in fluorescence microscopy with stimulated emission depletion beams of various shapes," *Phys. Rev. E. Stat. Phys. Plasmas Fluids Relat. Interdiscip. Top.*, vol. 64, pp. 066613-1–066613-9, 2001.

[5] S. W. Hell and M. Kroug, "Ground-state-depletion fluorescence microscopy: A concept for breaking the diffraction resolution limit," *Appl. Phys. B. Photophys. Laser Chem.*, vol. 60, pp. 495–497, 1995.

[6] R. Heintzmann, T. M. Jovin, and C. Cremer, "Saturated patterned excitation microscopy—A concept for optical resolution improvement," *J. Opt. Soc. Am. A, Opt. Image Sci.*, vol. 19, pp. 1599–1609, 2002.

[7] E. Betzig, G. H. Patterson, R. Sougrat, O. W. Lindwasser, S. Olenych, J. S. Bonifacino, M. W. Davidson, J. Lippincott-Schwartz, and H. F. Hess, "Imaging intracellular fluorescent proteins at nanometer resolution," *Science*, vol. 313, pp. 1642–1645, 2006.

[8] S. T. Hess, T. P. K. Girirajan, and M. D. Mason, "Ultra-high resolution imaging by fluorescence photoactivation localization microscopy," *Biophys. J.*, vol. 91, pp. 4258–4272, 2006.

[9] M. J. Rust, M. Bates, and X. Zhuang, "Sub-diffraction-limit imaging by stochastic optical reconstruction microscopy (STORM)," *Nat. Methods*, vol. 3, pp. 793–796, 2006.

[10] R. P. Goncalves, G. Agnus, P. Sens, C. Houssin, B. Bartenlian, and S. Scheuring, "Two-chamber AFM: Probing membrane proteins separating two aqueous compartments," *Nat. Methods*, vol. 3, pp. 1007–1012, 2006.

[11] D. J. Muller, D. Fotiadis, S. Scheuring, S. A. Muller, and A. Engel, "Electrostatically balanced subnanometer imaging of biological specimens by atomic force microscopy," *Biophys. J.*, vol. 76, pp. 1101–1111, 1999.

[12] F. A. Schabert, C. Henn, and A. Engel, "Native *Escherichia coli* OmpF porin surfaces probed by atomic force microscopy," *Science*, vol. 268, pp. 92–94, 1995.

[13] S. Scheuring and J. N. Sturgis, "Chromatic adaptation of photosynthetic membranes," *Science*, vol. 309, pp. 484–487, 2005.

[14] A. Harootunian, E. Betzig, M. S. Isaacson, and A. Lewis, "Super-resolution fluorescence near-field scanning optical microscopy," *Appl. Phys. Lett.*, vol. 49, pp. 674–676, 1986.

[15] D. W. Pohl, W. Denk, and M. Lanz, "Optical stethoscopy: Image recording with resolution l/20," *Appl. Phys. Lett.*, vol. 44, pp. 651–653, 1984.

[16] C. W. Hollars and R. C. Dunn, "Probing single molecule orientations in model lipid membranes with near-field scanning optical microscopy," *J. Chem. Phys.*, vol. 112, pp. 7822–7830, 2000.

[17] B. Hecht, H. Bielefeld, Y. Inouye, D. W. Pohl, and L. Novotny, "Facts and artifacts in near-field optical microscopy," *J. Appl. Phys.*, vol. 81, pp. 2492–2498, 1997.

[18] Y. C. Martin, H. F. Hamann, and H. K. Wickramasinghe, "Strength of the electric field in apertureless near-field optical microscopy," *J. Appl. Phys.*, vol. 89, pp. 5774–5778, 2001.

[19] J. Gersten and A. Nitzan, "Electromagnetic theory of enhanced Raman scattering by molecules adsorbed on rough surfaces," *J. Chem. Phys.*, vol. 73, pp. 3023–3037, 1980.

[20] P. F. Liao and A. Wokaun, "Lightning rod effect in surface enhanced Raman scattering," *J. Chem. Phys.*, vol. 76, pp. 751–752, 1982.

[21] J. N. Farahani, D. W. Pohl, H. J. Eisler, and B. Hecht, "Single quantum dot coupled to a scanning optical antenna: A tunable superemitter," *Phys. Rev. Lett.*, vol. 95, pp. 017402-1–017402-4, 2005.

[22] T. H. Taminiau, R. J. Moerland, F. B. Segerink, L. Kuipers, and N. F. V. Hulst, "λ/4 resonance of an optical monopole antenna probed by single molecule fluorescence," *Nano Lett.*, vol. 7, pp. 28–33, 2007.

[23] H. G. Frey, S. Witt, K. Felderer, and R. Guckenberger, "High-resolution imaging of single fluorescent molecules with the optical near-field of a metal tip," *Phys. Rev. Lett.*, vol. 93, pp. 200801-1–200801-4, 2004.

[24] J. M. Gerton, L. A. Wade, G. A. Lessard, Z. Ma, and S. R. Quake, "Tip-enhanced fluorescence microscopy at 10 nanometer resolution," *Phys. Rev. Lett.*, vol. 93, pp. 180801-1–180801-4, 2004.

[25] Z. Y. Ma, J. M. Gerton, L. A. Wade, and S. R. Quake, "Fluorescence near-field microscopy of DNA at sub-10 nm resolution," *Phys. Rev. Lett.*, vol. 97, pp. 260801-1–260801-4, 2006.

[26] C. Xie, C. Mu, J. R. Cox, and J. M. Gerton, "Tip-enhanced fluorescence microscopy of high-density samples," *Appl. Phys. Lett.*, vol. 89, pp. 143117-1–143117-3, 2006.

[27] H. F. Hamann, M. Kuno, A. Gallagher, and D. J. Nesbitt, "Molecular fluorescence in the vicinity of a nanoscopic probe," *J. Chem. Phys.*, vol. 114, pp. 8596–8609, 2001.

[28] A. Hartschuh, E. J. Sánchez, X. S. Xie, and L. Novotny, "High-resolution near-field raman microscopy of single-walled carbon nanotubes," *Phys. Rev. Lett.*, vol. 90, pp. 095503-1–095503-4, 2003.

[29] V. V. Protasenko, M. Kuno, A. Gallagher, and D. J. Nesbitt, "Fluorescence of single ZnS overcoated CdSe quantum dots studied by aperturelsss near-field scanning optical microscopy," *Opt. Commun.*, vol. 210, pp. 11–23, 2002.

[30] E. J. Sanchez, L. Novotny, G. R. Holtom, and X. S. Xie, "Room-temperature fluorescence imaging and spectroscopy of single molecules by two-photon excitation," *J. Phys. Chem. A*, vol. 101, pp. 7019–7023, 1997.

[31] E. J. Sanchez, L. Novotny, and X. S. Xie, "Near-field fluorescence microscopy based on two-photon excitation with metal tips," *Phys. Rev. Lett.*, vol. 82, pp. 4014–4017, 1999.

[32] T. J. Yang, G. A. Lessard, and S. R. Quake, "An apertureless near-field microscope for fluorescence imaging," *Appl. Phys. Lett.*, vol. 76, pp. 378–380, 2000.

[33] R. Hillenbrand, F. Keilmann, P. Hanarp, D. S. Sutherland, and J. Aizpurua, "Coherent imaging of nanoscale plasmon patterns with a carbon nanotube optical probe," *Appl. Phys. Lett.*, vol. 83, pp. 368–370, 2003.

[34] H. Gersen, M. F. García-Parajó, L. Novotny, J. A. Veerman, L. Kuipers, and N. F. van Hulst, "Influencing the angular emission of a single molecule," *Phys. Rev. Lett.*, vol. 85, pp. 5312–5315, 2000.

[35] L. Novotny, M. R. Beversluis, K. S. Youngworth, and T. G. Brown, "Longitudinal field modes probed by single molecules," *Phys. Rev. Lett.*, vol. 86, pp. 5251–5254, 2001.

[36] B. Sick, B. Hecht, and L. Novotny, "Orientational imaging of single molecules by annular illumination," *Phys. Rev. Lett.*, vol. 85, pp. 4482–4485, 2000.

[37] W. Trabesinger, A. Kramer, M. Kreiter, B. Hecht, and U. P. Wild, "Single-molecule near-field optical energy transfer microscopy," *Appl. Phys. Lett.*, vol. 81, pp. 2118–2120, 2002.

[38] D. Hu, M. Micic, N. Klymyshyn, Y. D. Suh, and H. P. Lu, "Correlated topographic and spectroscopic imaging beyond diffraction limit by atomic force microscopy metallic tip-enhanced near-field fluorescence lifetime microscopy," *Rev. Sci. Inst.*, vol. 74, pp. 3347–3355, 2003.

[39] P. Anger, P. Bharadwaj, and L. Novotny, "Enhancement and quenching of single-molecule fluorescence," *Phys. Rev. Lett.*, vol. 96, pp. 113002-1–113002-4, 2006.

[40] L. Novotny, R. X. Bian, and X. S. Xie, "Theory of nanometric optical tweezers," *Phys. Rev. Lett.*, vol. 79, pp. 645–648, 1997.

[41] H. G. Frey, F. Keilmann, A. Kriele, and R. Guckenberger, "Enhancing the resolution of scanning near-field optical microscopy by a metal tip grown on an aperture probe," *Appl. Phys. Lett.*, vol. 81, pp. 5030–5032, 2002.

[42] R. Saito, G. Dresselhaus, and M. S. Dresselhaus, *Physical Properties of Carbon Nanotubes*. London, U.K.: Imperial College Press, 1998.

[43] J. F. Hafner, C.-L. Cheung, T. H. Oosterkamp, and C. M. Leiber, "High-yield assembly of individual single-walled carbon nanotube tips for scanning probe microscopies," *J. Phys. Chem. B*, vol. 105, pp. 743–746, 2001.

[44] L. Wade, I. Shapiro, Z. Ma, S. Quake, and C. P. Collier, "Correlating AFM probe morphology to image resolution for single-wall carbon nanotube tips," *Nano Lett.*, vol. 4, pp. 725–731, 2004.

[45] R. Dorn, S. Quabis, and G. Leuchs, "Sharper focus for a radially polarized light beam," *Phys. Rev. Lett.*, vol. 91, pp. 233901-1–233901-4, 2003.

[46] L. G. Schulz, "The optical constants of silver, gold, copper, and aluminum I. The absorption coefficient k," *J. Opt. Soc. Am.*, vol. 44, pp. 357–362, 1954.

[47] E. D. Palik, *Handbook of Optical Constants of Solids*. Orlando, FL: Academic, 1985.

[48] S. Adachi, "Model dielectric constants of Si and Ge," *Phys. Rev. B, Condens. Matter*, vol. 38, pp. 12966–12976, 1988.

[49] J. Humlicek, M. Garriga, M. I. Alonso, and M. Cardona, "Optical spectra of Si_xGe_{1-x} alloys," *J. Appl. Phys.*, vol. 65, pp. 2827–2832, 1989.

[50] K. Kempa, J. Rybczynski, Z. P. Huang, K. Gregorczyk, A. Vidan, B. Kimball, J. Carlson, G. Benham, Y. Wang, A. Herczynski, and Z. F. Ren, "Carbon nanotubes as optical antennae," *Adv. Mater.*, vol. 19, pp. 421–426, 2007.

[51] Y. Lan, B. Q. Zeng, H. Zhang, B. R. Chen, and Z. H. Yang, "Simulation of carbon nanotube THz antenna arrays," *Int. J. Infrared Millm. Waves*, vol. 27, pp. 871–877, 2006.

[52] G. Y. Slepyan, M. V. Shuba, S. A. Maksimenko, and A. Lakhtakia, "Theory of optical scattering by achiral carbon nanotubes and their potential as optical nanoantennas," *Phys. Rev. B, Condens. Matter*, vol. 73, pp. 195416-1–195416-11, 2006.

[53] M. S. Dresselhaus, "Nanotube antennas," *Nature*, vol. 432, pp. 959–960, 2004.

[54] A. Jorio, A. G. Souza, V. W. Brar, A. K. Swan, M. S. Unlu, B. B. Goldberg, A. Righi, J. H. Hafner, C. M. Lieber, R. Saito, G. Dresselhaus, and M. S. Dresselhaus, "Polarized resonant Raman study of isolated single-wall carbon nanotubes: Symmetry selection rules, dipolar and multipolar antenna effects," *Phys. Rev. B, Condens. Matter*, vol. 65, pp. 121402-1–121402-4, 2002.

[55] Y. Wang, K. Kempa, B. Kimball, J. B. Carlson, G. Benham, W. Z. Li, T. Kempa, J. Rybczynski, A. Herczynski, and Z. F. Ren, "Receiving and transmitting light-like radio waves: Antenna effect in arrays of aligned carbon nanotubes," *Appl. Phys. Lett.*, vol. 85, pp. 2607–2609, 2004.

[56] E. S. Snow, P. M. Campbell, and J. P. Novak, "Single-wall carbon nanotube atomic force microscope probes," *Appl. Phys. Lett.*, vol. 80, pp. 2002–2004, 2002.

[57] N. R. Wilson, D. H. Cobden, and J. V. Macpherson, "Single-wall carbon nanotube conducting probe tips," *J. Phys. Chem. B*, vol. 106, pp. 13102–13105, 2002.

[58] J. S. Bunch, T. N. Rhodin, and P. L. McEuen, "Noncontact-AFM imaging of molecular surfaces using single-wall carbon nanotube technology," *Nanotechnol.*, vol. 15, pp. S76–S78, 2004.

[59] M. J. Esplandiu, V. G. Bittner, P. G. Konstantinos, and C. P. Collier, "Nanoelectrode scanning probes from fluorocarbon-coated single walled carbon nanotubes," *Nano Lett.*, vol. 4, pp. 1873–1879, 2004.

[60] A. Patil, J. Sippel, G. W. Martin, and A. G. Rinzler, "Enhanced functionality of nanotube atomic force microscopy tips by polymer coating," *Nano Lett.*, vol. 4, pp. 303–308, 2004.

[61] Q. Ye, A. M. Cassell, H. B. Liu, K. J. Chao, J. Han, and M. Meyyappan, "Large-scale fabrication of carbon nanotube probe tips for atomic force microscopy critical dimension Imaging applications," *Nano Lett.*, vol. 4, pp. 1301–1308, 2004.

[62] D. P. Burt, N. R. Wilson, J. M. R. Weaver, P. S. Dobson, and J. V. Macpherson, "Nanowire probes for high resolution combined scanning electrochemical microscopy—Atomic force microscopy," *Nano Lett.*, vol. 5, pp. 639–643, 2005.

[63] S. Carnally, K. Barrow, M. R. Alexander, C. J. Hayes, S. Stolnik, S. J. B. Tendler, P. M. Williams, and C. J. Roberts, "Ultra-resolution imaging of a self-assembling biomolecular system using robust carbon nanotube AFM probes," *Langmuir*, vol. 23, pp. 3906–3911, 2007.

[64] A. Krishnan, E. Dujardin, T. W. Ebbesen, P. N. Yianilos, and M. M. J. Treacy, "Young's modulus of single-walled nanotubes," *Phys. Rev. B, Condens. Matter*, vol. 58, pp. 14013–14019, 1998.

[65] M. M. J. Treacy, T. W. Ebbesen, and J. M. Gibson, "Exceptionally high Young's modulus observed for individual carbon nanotubes," *Nature*, vol. 381, pp. 678–680, 1996.

[66] C. L. Cheung, J. F. Hafner, and C. M. Leiber, "Carbon nanotube atomic force microscopy tips: Direct growth by chemical vapor deposition and application to high-resolution imaging," *Proc. Natl. Acad. Sci. U.S.A*, vol. 97, pp. 3809–3813, 2000.

[67] L. Wade, I. Shapiro, Z. Ma, S. Quake, and C. P. Collier, "Single-molecule fluorescence and force microscopy employing carbon nanotubes," *Nanotechnol.*, vol. 3, pp. 317–320, 2003.

[68] I. Shapiro, S. D. Solares, M. J. Esplandiu, L. Wade, W. Goddard, and C. P. Collier, "Influence of elastic deformation on single-wall carbon nanotube atomic force microscopy probe resolution," *J. Phys. Chem. B*, vol. 108, pp. 13613–13618, 2004.

[69] L. Chen, C.-L. Cheung, P. D. Ashby, and C. M. Leiber, "Single-walled carbon nanotube AFM probes: Optimal imaging resolution of nanoclusters and biomolecules in ambient and fluid environments," *Nano Lett.*, vol. 4, pp. 1725–1731, 2004.

[70] D. B. Asay and S. H. Kim, "Effects of adsorbed water layer structure on adhesion force of silicon oxide nanoasperity contact in humid ambient," *J. Chem. Phys.*, vol. 124, pp. 174712-1–174712-5, 2006.

[71] K. Karrai and I. Tiemann, "Interfacial shear force microscopy," *Phys. Rev. B, Condens. Matter*, vol. 62, pp. 174–181, 2000.

[72] M. C. Strus, A. Raman, C.-S. Han, and C. V. Nguyen, "Imaging artefacts in atomic force microscopy with carbon nanotube tips," *Nanotechnol.*, vol. 16, pp. 2482–2492, 2005.

[73] A. Mechler, J. Kopinczky, J. Kokavecz, A. Hoel, C.-G. Granqvist, and P. Heszler, "Anomalies in nanostructure size measurements by AFM," *Phys. Rev. B, Condens. Matter*, vol. 72, pp. 125407-1–125407-6, 2005.

[74] F. M. Huang, F. Culfaz, F. Festy, and D. Richards, "Effect of the surface water layer on the optical signal in apertureless scanning near field optical microscopy," *Nanotechnol.*, vol. 18, pp. 015501-1–015501-3, 2007.

[75] S. Davy, M. Spajer, and D. Courjon, "Influence of the water layer on the shear force damping in near-field microscopy," *Appl. Phys. Lett.*, vol. 73, pp. 2594–2596, 1998.

[76] J. Freund, J. Halbritter, and J. K. H. Horber, "How dry are dried samples? Water adsorption measured by STM," *Microsc. Res. Tech.*, vol. 44, pp. 327–338, 1999.

[77] T. Stifter, O. Marti, and B. Bhushan, "Theoretical investigation of the distance dependence of capillary and van der Waals forces in scanning force microscopy," *Phys. Rev. B, Condens. Matter*, vol. 62, pp. 13667–13673, 2000.

[78] P. K. Wei and W. S. Fann, "The effect of humidity on probe-sample interactions in near-field scanning optical microscopy," *J. Appl. Phys.*, vol. 87, pp. 2561–2564, 2000.

[79] S. D. Solares, M. J. Esplandiu, W. Goddard, and C. P. Collier, "Mechanisms of single-walled carbon nanotube probe-sample multistability in tapping mode AFM imaging," *J. Phys. Chem. B*, vol. 109, pp. 11493–11500, 2005.

[80] V. Biju, T. Itoh, Y. Baba, and M. Ishikawa, "Quenching of photoluminescence in conjugates of quantum dots and single-walled carbon nanotube," *J. Phys. Chem. B*, vol. 110, pp. 26068–26074, 2006.
[81] T. G. Hedderman, S. M. Keogh, G. Chambers, and H. J. Byrne, "Solubilization of SWNTs with organic dye molecules," *J. Phys. Chem. B*, vol. 108, pp. 18860–18865, 2004.
[82] Y. Tomonari, H. Murakami, and N. Nakashima, "Solubilization of single-walled carbon nanotubes by using polycyclic aromatic ammonium amphiphiles in water—Strategy for the design of high-performance solubilizers," *Chem. Eur. J.*, vol. 12, pp. 4027–4034, 2006.
[83] J. Müller, J. M. Lupton, A. L. Rogach, J. Feldmann, D. V. Talapin, and H. Weller, "Air-induced fluorescence bursts from single semiconductor nanocrystals," *Appl. Phys. Lett.*, vol. 85, pp. 381–383, 2004.

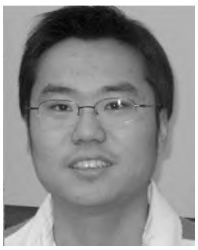

Chun Mu received the B.S. degree in physics from the University of Science and Technology of China, Hefei, China, in 2003. He is currently working toward the Ph.D. degree in physics in the Department of Physics, University of Utah, Salt Lake City, as part of Jordan Gerton's Nano-Optics Group.

Benjamin D. Mangum received the B.A. degree in physics from the Department of Physics, University of Utah, Salt Lake City, in 2004, where he is currently working toward the Ph.D. degree in physics, as part of Jordan Gerton's Nano-Optics Group.

Changan Xie received the Ph.D. degree in biomedical physics from East Carolina University, Greenville, NC, in 2004.

In 2005, he joined the Gerton Laboratory, Department of Physics, University of Utah. He is currently with the Department of Biochemistry and Molecular Biology, Georgetown University, Washington, DC.

Jordan M. Gerton received the Ph.D. degree in physics from Rice University, Houston, TX, in 2001.

In 2001, he joined Stephen Quake's Biophysics Group at the California Institute of Technology. In 2003, he was appointed a Beckman Senior Research Fellow. In 2004, he joined the Department of Physics, University of Utah, Salt Lake City, where he is currently an Assistant Professor of Physics and Adjunct Assistant Professor of Bioengineering. His current research interests include nano-optics and molecular biophysics.